Nuclear Instruments and Methods in Physics Research B 267 (2009) 3072–3075

Contents lists available at ScienceDirect

Nuclear Instruments and Methods in Physics Research B

journal homepage: www.elsevier.com/locate/nimb

Surface amorphization, sputter rate, and intrinsic stresses of silicon during low energy Ga^+ focused-ion beam milling

Lars Pastewka [a,c], Roland Salzer [b], Andreas Graff [b], Frank Altmann [b], Michael Moseler [a,c,d,*]

[a] Fraunhofer-Institut für Werkstoffmechanik IWM, Wöhlerstraße 11, 79108 Freiburg, Germany
[b] Fraunhofer-Institut für Werkstoffmechanik IWM, Walter-Hülse-Straße 1, 06120 Halle, Germany
[c] Physikalisches Institut, Universität Freiburg, Hermann-Herder-Straße 3, 79104 Freiburg, Germany
[d] Freiburger Materialforschungszentrum, Stefan-Meier-Straße 21, 79104 Freiburg, Germany

ARTICLE INFO

Article history:
Available online 18 June 2009

PACS:
61.43.Dq
61.80.Az
61.80.Jh
61.82.Fk
81.40.Wx

Keywords:
Surface amorphization
Focused ion beam milling
Molecular dynamics
Silicon

ABSTRACT

Transmission electron microscopy (TEM) is a standard technique to characterize microelectronic device structures. As structures shrink to the nanoscale, surface damage produced by focused ion beam (FIB) sample preparation destroying the region of interest and degrading the resolution of TEM images becomes increasingly a problem. The thickness of the damaged layer at the sidewalls of a prepared cross section is around 20–30 nm for silicon at typical beam energies of 30 keV. In order to reduce these artifacts to a minimum low beam energies have been proposed for FIB polishing. We use a combination of molecular dynamics simulations and experiments to assess the influence of the focused ion beam on the surface structure of silicon for beam energies ranging from 1–5 keV and a grazing angle of 10° typically used in low voltage FIB polishing. Under these conditions, the thickness of the amorphous layer depends linearly on the beam energy. Intrinsic surface stresses introduced by FIB are always tensile and of a magnitude of around 1 GPa.

1. Introduction

FIB milling has become one of the most important tools for micro- and nanostructuring of substrates, and for preparation of samples for scanning electron microscopy and TEM cross section analysis [1,2]. Even though its precision supersedes almost all other techniques the surface is still damaged on the nanometer scale [3]. Intrinsic stresses introduced in the damaged surface layer could lead to a buckling of the structures, an effect which has been studied in some detail for alumina [4,5]. A possibility to produce surfaces of higher quality is to lower the beam energy [6,7].

In this study, we elaborate the influence of a focused ion beam on an ideal silicon surface using molecular dynamics (MD) simulations. Previous work has focused on single impact events [8–12], sputtering silicon using argon ions [13–17] and stresses [18]. For a review on the topic see [19]. In contrast to sputtering, FIB milling involves very low grazing impact angles which have so far only been studied using very small sample sizes [20]. Additional FIB milling experiments validate the reliability of our simulations.

2. Computational method

The silicon–silicon interaction is computed using the Tersoff III potential [21]. For the gallium–silicon interaction we use the potential of Ziegler, Biersack and Littmark (ZBL) [22]. The time step is dynamically adjusted up to a maximum of 1 fs to maintain a maximum displacement of 0.05 Å per MD step in order to properly sample peak pressures and thermal spikes.

The gallium ions are incident on the surface at a randomly chosen impact position. Around the impact position at a distance of 1.8 nm parallel to the ion's path the atoms are thermalized to 300 K using a Langevin thermostat (see inset in Fig. 1) whose dissipation constant is set to 0.044 fs^{-1} as derived from the Debye frequency of silicon [23]. This ensures proper dissipation of the impact energy. Furthermore, the bottom 1 nm of each slab of silicon are held at a fixed position and the following 1 nm are also thermalized using the parameters given above. Initially, the gallium ion is placed at a distance of 1 nm above the surface of the slab. The trajectory is then followed for 15 ps. Note that the temperature of the whole slab has reached 300 K after circa 10 ps. Since the ZBL potential reflects only short ranged core repulsion and not covalent bonds with the surrounding silicon, we consider two cases: First, we completely remove the gallium leaving a

* Corresponding author. Address: Physikalisches Institut, Universität Freiburg, Hermann-Herder-Straße 3, 79104 Freiburg, Germany.
E-mail address: michael.moseler@iwm.fraunhofer.de (M. Moseler).

0168-583X/$ - see front matter © 2009 Elsevier B.V. All rights reserved.
doi:10.1016/j.nimb.2009.06.094

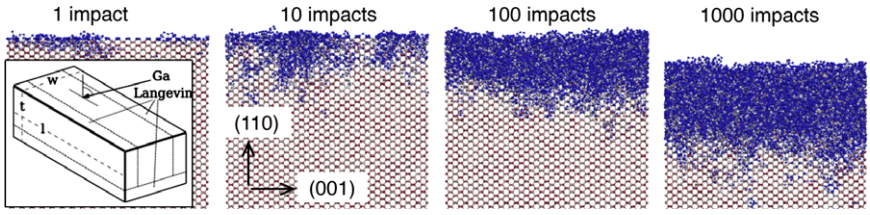

Fig. 1. Snapshots of the (1 1 0) surface after 1, 10, 100 and 1000 impacts with an energy of 2 keV at an angle of 80°. Red atoms are in a diamond whereas blue atoms are in an amorphous environment. Inset: Simulation setup. The sketch shows the thermalized regions. Additionally, the very bottom 1 nm of atoms is held fixed. (For interpretation of the references to colour in this figure legend, the reader is referred to the web version of this article.)

vacancy behind, and second, we leave the gallium as is and continue computing the interaction using the ZBL potential. This represents two limiting cases: The vacancy introduces a local tensile stress while the ZBL potential introduces a compressive stress due to its repulsive nature. In all cases we find that the general results—thickness of the amorphous layer, sputter rate and intrinsic stress—are insensitive to the method employed. This indicates that the subplanted gallium has no influence on the film's properties. All results shown in the following are taken from the first case.

The local crystal structure of the material is determined by computing coordination fingerprints $\vec{Q}_i$ for each atom i given by [24]

$$Q_i^{(l)} = \frac{1}{Z_i}\left(\sum_{j\neq i}\sum_{k\neq i} P^{(2l)}(\cos\theta_{jik})\right)^{\frac{1}{2}}, \quad (1)$$

where $P^{(l)}(x)$ is the Legendre polynomial and Z_i the local coordination of atom i. The sum is taken over neighbors within a cut-off of 2.6 Å. For the diamond structure one finds $Q_D^{l=1\ldots6} = (0.0, 0.509, 0.629, 0.213, 0.650, 0.415)$. An atom is defined to be in a diamond environment if the cartesian distance obeys $|\vec{Q} - \vec{Q}_D| < 0.2$. Furthermore, we define the position of the interface between the amorphous layer and the crystalline zone to the position where the number of atoms in a diamond environment has dropped to 50%.

Stress is determined via the virial [25]. While the total virial can be computed straightforwardly [26], there exists no unambiguous partitioning scheme which assigns a virial contribution to each atom. When averaging over sufficiently large slices of volume this problem vanishes [27]. All stresses are obtained by averaging over a 10 ps MD run of the final configuration at 300 K.

3. Experimental method

The simulations are compared to TEM investigations on a silicon single crystal irradiated with Ga^+ ions of different energies. Here, trenches of a depth of 5 µm are milled into a single crystal silicon H-bar (see Fig. 2(a) and [2] for TEM target preparation). The cross-sections are then polished with 2, 5, 10, 20 and 30 kV Ga^+ beams. Assisted by the electron beam a platinum bar is deposited to protect the polished cross-sections. For high resolution TEM investigations an electron transparent lamella is prepared showing a lateral cut of the protected polished cross-sections (see Fig. 2(b)). The thickness of the amorphous layer can then be straightforwardly determined from TEM images (see Figs. 2(c) and 2(d)).

4. Thickness of the amorphous layer and sputter rate

The simulations start from an initially perfect slab of crystalline silicon. Ion energies of 1, 2 and 5 keV are used at an incident angle of 80° for the silicon (1 1 0) surface. We check the influence of crystal orientation by comparing with results for the (1 0 0) and (1 1 1) surface using 2 keV beam energy. Furthermore, at 2 keV and on the (1 1 0) surface we perform additional simulations at incident angles of 0° and 40°. The sizes of the initial samples are summarized in Table 1.

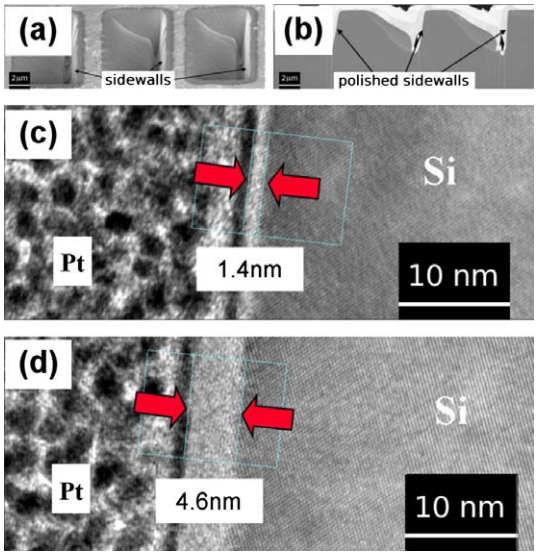

Fig. 2. TEM sample preparation and thickness of the amorphous layer: (a) Trenches prepared by FIB, (b) cross-sections of the platinum-protected sidewalls, (c) and (d) TEM images of the interface between protective platinum-coating and the silicon single crystal, polished with 2 and 5 kV beams, respectively.

Snapshots of the sample after 1, 10, 100, and 1000 impacts are shown in Fig. 1. Already a single impact induces significant surface damage over an area which is not only localized at the impact position. Point defects within the bulk of the material are observed after 100–1000 impacts. While no line or areal defects are observed this is most likely due to the finite size of the system which inhibits the formation of extended defects. Furthermore, around 25%, 40% and 50% of the ions are implanted in the 1, 2 and 5 keV case. For 2 keV ions at an angle of 40° we already observe 98% implantation.

Fig. 3(a) shows the evolution of the interface between the amorphous surface layer and the crystalline bulk silicon as a function of impacts per surface area. After a certain number of impacts the interface is in a steady-state situation which means that the amorphous interface progresses at the same pace as the surface

Table 1
Configurations used for the FIB simulations. Thickness (t) denotes the total sample thickness, length (l) the size of the sample in direction of the Ga^+ and width (w) the perpendicular dimension (see inset Fig. 1). The last column gives the total number of atoms in each sample.

Surface	Ga^+	t (nm)	l (nm)	w (nm)	Atoms
(1 1 0)	[0 0 1]	22.5	10.9	5.4	62720
(1 1 1)	$[1\,1\,\bar{2}]$	22.8	10.6	5.4	64512
(1 0 0)	[0 1 0]	24.9	10.9	5.4	70400

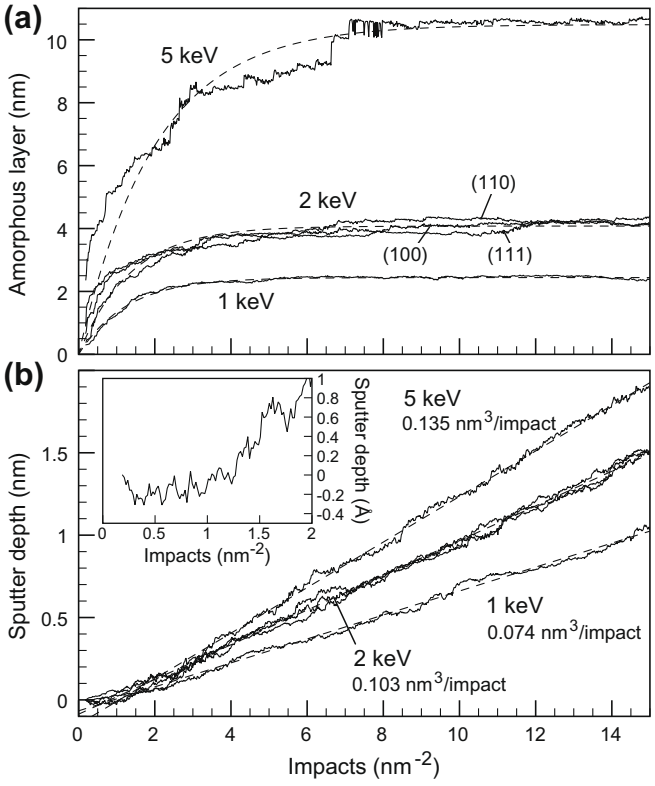

Fig. 3. (a) Evolution of the amorphous layer as a function of impacts for different beam energies and different surface orientations. No influence of the surface orientation on the thickness can be observed. The dashed lines are exponential fits to the data used to extract the steady-state interface thickness. (b) Sputter depth as a function of impacts per surface area. The inset shows a blow up of the 5 keV curve in the main panel.

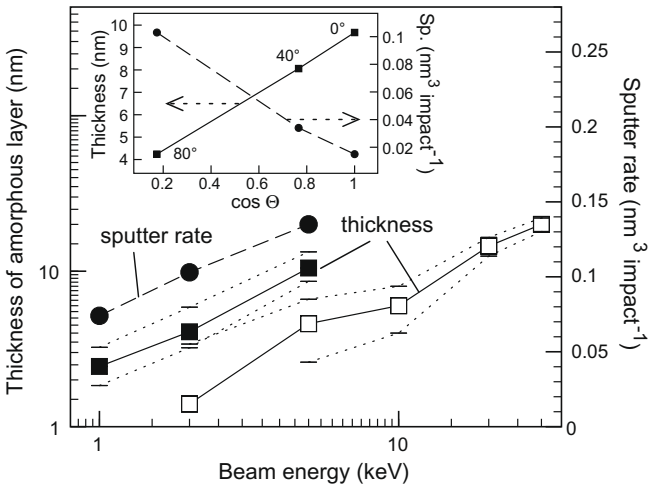

Fig. 4. Thickness of the amorphous layer and sputter rate as a function of beam energy. Solid symbols denote simulation results while open symbols show measurements. The error bars for the theoretical layer thickness have been determined from 10% and 90% threshold values (symbols 50%, see text). Experimentally, an error of approximately 2 nm has been extracted by measuring the layer thickness at different positions in one sample. Inset: Thickness and sputter rate as a function of incident angle θ at 2 keV (simulation results).

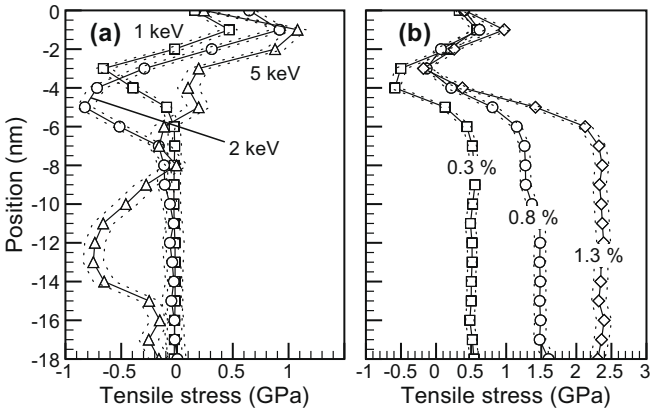

Fig. 5. Intrinsic stress in the milled 110 surface as a function of depth: (a) in dependence on impact energy and (b) in dependence on pre-strain for 2 keV ions. The dashed lines indicate the fluctuation of the average stress during an MD run (one standard deviation).

is sputtered. Clearly, the steady-state thickness of the amorphous layer shows a dependence on the kinetic energy of the incident ion. An influence of the crystal orientation on the thickness of the amorphous layer cannot be detected within the accuracy of the simulation. The steady-state interface thickness is extracted by fitting an exponential to the data—see dashed line in Fig. 3(a).

The sputter rate for the different setups is shown in Fig. 3(b). An almost perfect linear dependence of the thickness of the sputtered layer on the number of impacts is found. Again, the surface orientation does not influence the sputter rate as the steady-state surface "seen" by the Gallium ions is always amorphous. The inset in Fig. 3(b) shows the initial stage of the 5 keV simulation. Interestingly, the interface initially advances (negative sputter depth). This is due to heavy surface amorphization reducing the density of the initially crystalline silicon.

High resolution TEM images of the interface between the platinum-protection layer and the silicon single crystal (see Figs. 2(c) and 2(d)) allow to measure the thickness of the amorphous layer. These results as well as the steady-state thickness of the amorphous zone and the steady-state sputter rate as obtained from the simulations are shown as a function of beam energy in Fig. 4. Here, an almost linear dependence of the layer thickness on the beam energy is found. An approximately logarithmic dependence is found for the sputter rate which thus scales sub-linearly with beam energy.

5. Intrinsic stresses

FIB milling introduces stresses into the amorphous surface layer. Fig. 5(a) shows the tensile stress profile as function of depth. In all cases, the peak stress is around 1 GPa, tensile at the surface and compressive at the amorphous–crystalline interface.

Modern silicon electronics uses pre-strained substrates in order to increase the electron mobility. In order to check the influence of pre-strain on FIB preparation we strain the lattice isotropically at 0.3%, 0.8% and 1.3%. The depth profiles are shown in Fig. 5(b). While pre-straining does not affect the thickness of the amorphous layer as well as the sputter rate the intrinsic stresses are changed dramatically. A strain of 0.3% introduces a tensile homogeneous stress of approximately 0.5 GPa which matches the stress introduced by the surface amorphization.

6. Discussion and conclusions

Fig. 4 summarizes the main results of this work. The simulations suggest, that the thickness of the amorphous film increases linearly with beam energy while the sputter rate shows a logarithmic dependence in the energy range that is investigated. Experimental thicknesses follow the simulation's trends, however they

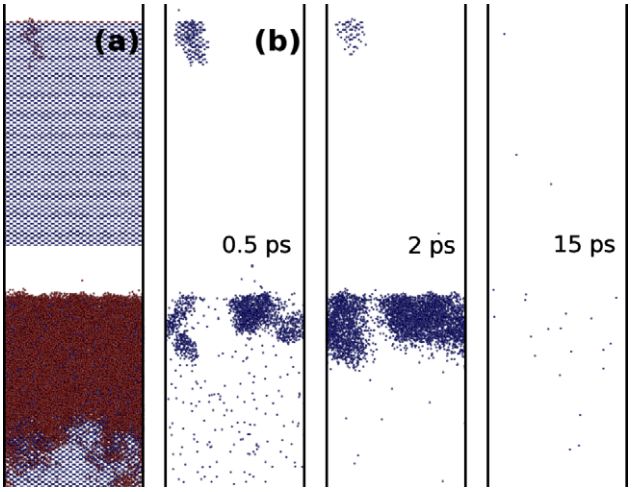

Fig. 6. Snapshots of a single impact simulation at 5 keV. Top: First impact on the pristine surface, bottom: impact on the steady-state amorphous surface. In both cases the gallium is ejected from the surface at thermal velocities. Shown are the: (a) final atomic configurations and (b) atoms with a kinetic energy above 1000 K.

lie below the simulated ones. This can have a number of reasons: First of all, we expect recrystallization of parts of the amorphous layer. At experimental beam currents of approximately 500 pA and a spot sizes of around 5 μm the experimental beam intensity is six orders of magnitude smaller than the one used in the simulation. Since no significant heating which speeds up recrystallization is observed in the simulation we expect only slow recrystallization in the experiment. Secondly, under experimental conditions it is difficult to control the exact angle of the incident beam. Due to surface topography, the ions will locally hit the surface at different angles. At low grazing incidence a minimal change of angle will lead to a large change in momentum which is transfered *perpendicular* to the surface. This is exemplarily shown in the inset of Fig. 4. The film thickness scales approximately linear with the cosine of the incident angle which indicates that indeed the momentum and not the energy carried perpendicular to the surface is relevant. Thus, at 80° a variation of ±5° can lead to a change in thickness of ±50% and is thus the most likely source of the difference.

In order to describe stress formation in irradiated surfaces heat spike models have been proposed [28] and described using continuum theory [29]. These spikes are known to create tensile stresses for high beam energies in metals [30,31] which are attributable to solidification of a locally melted zone to a glassy state. Fig. 6 shows that there is always a localized region which is hotter than the glass transition temperature of amorphous silicon (about 1000 K, see [32]). An outflow of the material is also indicated by the initial negative sputter rates shown in the inset of Fig. 3(b).

In summary, as advice for FIB practitioners one might state: because the sputter rate scales sublinear it is beneficial to operate at beam energies where the sputter rate is sufficient and the surface amorphization is tolerable. Increasing the beam energy will more quickly lead to a low quality surface structure while the sputter rate increases only marginally.

References

[1] J. Mayer, L.A. Giannuzzi, T. Kamino, J. Michael, MRS Bull. 32 (2007) 400.
[2] F. Altmann, Prakt. Metallogr. 42 (2005) 206.
[3] S. Rubanov, P.R. Munroe, J. Microsc. Oxford 214 (2004) 213.
[4] F. Elfallagh, B.J. Inkson, J. Microsc. Oxford 230 (2008) 240.
[5] B.J. Inkson, D. Leclere, F. Elfallagh, B. Derby, J. Phys.: Conf. Ser. 26 (2006) 219.
[6] F. Altmann, A. Graff, M. Simon, H. Hoffmeister, P. Gnauck, Prakt. Metallogr. 43 (2006) 396.
[7] N.I. Kato, J. Electron. Microsc. 53 (2004) 451.
[8] K. Nordlund, M. Ghaly, R.S. Averback, M. Caturla, T.D. de la Rubia, J. Tarus, Phys. Rev. B 57 (1998) 7556.
[9] M.-J. Caturla, T.D. de la Rubia, L.A. Marquéz, G.H. Gilmer, Phys. Rev. B 54 (1996) 16683.
[10] T.D. de la Rubia, G.H. Gilmer, Phys. Rev. Lett. 74 (1995) 2507.
[11] D.M. Stock, G.H. Gilmer, M. Jaraíz, T.D. de la Rubia, Nucl. Instr. and Meth. B 102 (1995) 207.
[12] R. Smith, D.E. Harrison Jr., B.J. Garrison, Phys. Rev. B 40 (1989) 93.
[13] M. Timonova, B.-J. Lee, B.J. Thijsse, Nucl. Instr. and Meth. B 255 (2007) 195.
[14] B.J. Thijsse, T.P.C. Klaver, E.F.C. Haddeman, Appl. Surf. Sci. 231 (2004) 29.
[15] M.C. Moore, N. Kalyanasundaram, J.B. Freund, H.T. Johnson, Nucl. Instr. and Meth. B 225 (2004) 241.
[16] E.F.C. Haddeman, B.J. Thijsse, Nucl. Instr. and Meth. B 202 (2003) 161.
[17] J.E. Rubio, L.A. Marqués, L. Pelaz, M. Jaraiz, J. Barbolla, Nucl. Instr. and Meth. B 112 (1996) 156.
[18] K.M. Beardmore, N. Grønbech-Jensen, Phys. Rev. B 60 (1999) 12610.
[19] L. Pelaz, L.A. Marqués, J. Barbolla, J. Appl. Phys. 96 (2004) 5947.
[20] L.A. Giannuzzia, B.J. Garrison, J. Vac. Sci. Technol. A 25 (2007) 1417.
[21] J. Tersoff, Phys. Rev. B 38 (1988) 9902.
[22] J. Ziegler, J. Biersack, U. Littmark, The Stopping and Range of Ions in Matter, Pergamon Press, 1985.
[23] S.A. Adelman, J.D. Doll, J. Chem. Phys. 64 (1976) 2375.
[24] B.J. Thijsse, Private communication, A simplified version of this method is described in: P.J. Steinhardt, D.R. Nelson, M. Ronchetti, Phys. Rev. B 28 (1983) 784.
[25] M.P. Allen, D.J. Tildesley, Computer Simulation of Liquids, Clarendon Press, 1989.
[26] J.E. Carpenter, J. Comput. Chem. 23 (2002) 667.
[27] A.Y. Belov, H.U. Jäger, Comp. Mater. Sci. 24 (2002) 154.
[28] T.D. de la Rubia, R.S. Averback, R. Benedek, W.E. King, Phys. Rev. Lett. 59 (1987) 1930.
[29] H. Trinkaus, A.I. Ryazanov, Phys. Rev. Lett. 74 (1995) 5072.
[30] W.-L. Chan, K. Zhao, N. Vo, Y. Ashkenazy, D.G. Cahill, R.S. Averback, Phys. Rev. B 77 (2008) 205405.
[31] S.G. Mayr, R.S. Averback, Phys. Rev. B 68 (2003) 214105.
[32] A. Hedler, S.L. Klaumünzer, W. Wesch, Nat. Mater. 3 (2004) 804.